Available online at www.sciencedirect.com
SCIENCE DIRECT
Journal of Asian Earth Sciences 27 (2006) 207–222
Journal of Asian Earth Sciences
www.elsevier.com/locate/jaes

Kinematic development and paleostress analysis of the Denizli Basin (Western Turkey): implications of spatial variation of relative paleostress magnitudes and orientations

Nuretdin Kaymakci*

RS/GIS Laboratory, Department of Geological Engineering, Middle East Technical University 06531 Ankara, Turkey

Received 17 November 2004; accepted 19 March 2005

Abstract

Paleostress orientations and relative paleostress magnitudes (stress ratios), determined by using the reduced stress concept, are used to improve the understanding of the kinematic characteristics of the Denizli Basin. Two different dominant extension directions were determined using fault-slip data and travertine fissure orientations. In addition to their stratigraphically coeval occurrence, the almost exact fit of the σ_2 and σ_3 orientations for the NE–SW and NW–SE extension directions in the Late Miocene to Recent units indicate that these two extension directions are a manifestation of stress permutations in the region and are contemporaneous. This relationship is also demonstrated by the presence of actively developing NE–SW and NW–SE elongated grabens developed as the result of NE–SW and NW–SE directed extension in the region. Moreover, stress ratios plots indicate the presence of a zone of major stress ratio changes that are attributed to the interference of graben systems in the region. It is concluded that the plotting of stress orientations and distribution of stress ratios is a useful tool for detecting major differences in stress magnitudes over an area, the boundaries of which may indicate important subsurface structures that cannot be observed on the surface.

Keywords: Paleostress; Relative stress magnitudes; Stress permutation; Denizli basin; Turkey

1. Introduction

The state of stress in rocks is generally anisotropic and is defined by stress ellipsoid axes, which characterize the magnitudes of the principal stresses. In positive compression, the longest axis is the ellipsoid's major stress (σ_1), the intermediate axis is the intermediate stress (σ_2), and the shortest axis is the minimum stress (σ_3) (Jaeger and Cook, 1969, p. 11–20). The orientation and shape of the stress ellipsoid with respect to earth's surface controls the type, orientation and slip sense of faults developed in an area (Angelier, 1994). For this purpose, a number of paleostress inversion methods have been developed using graphical (e.g. Arthaud, 1969; Angelier, 1984; Krantz, 1988) and analytical means (Carey and Brunier, 1974; Etchecopar et al., 1981; Angelier et al., 1982; Armijo et al., 1982; Gephart and Forsyth, 1984; Michael, 1984; Carey-Gailhardis and Mercier, 1987; Reches, 1987; Angelier, 1990; Gephart, 1990; Marrett and Almandinger, 1990; Will and Powell, 1991; Yin and Ranalli, 1993). Over the last three decades, paleostress inversion techniques have been applied to various tectonic settings and have proved to be empirically valid and successful, despite the fact that there are certain limitations (Pollard et al., 1993; Nemcok and Lisle, 1997; Twiss and Unruh, 1998). Furthermore, paleostress inversion studies are also used to determine the effect of past slip events along active faults by making use of deflections in the orientations of the stress axes to recognize stress perturbations near the major faults (Homberg et al., 1997, Homberg et al., 2004). Most of the analytical methods apply the Wallace (1951) and Bott (1959) assumption, which states that slip occurs parallel to the maximum resolved shear stress on a pre-existing and/or newly formed fault plane. Using this assumption, and

* Tel.: +90 312 210 26 85; fax: +90 312 210 12 63.
E-mail address: kaymakci@metuedu.tr

1367-9120/$ - see front matter © 2005 Elsevier Ltd. All rights reserved.
doi:10.1016/j.jseaes.2005.03.003

reversing it, Angelier (1975) proposed the 'reduced stress tensor' concept and stress ratio [$\Phi = (\sigma_2 - \sigma_3)/(\sigma_1 - \sigma_3)$] which describes the shape of the stress ellipsoid from which ratios of principal paleostress magnitudes can be calculated. However, determination of absolute magnitudes from natural examples of fault-slip data is possible to some extent (Bergerat, 1987; Angelier, 1989; André et al., 2001), but is generally very difficult, due to a number of unknowns related to the environmental conditions during faulting that cannot be obtained from fault-slip data alone. Therefore, the standard paleostress inversion techniques are used only for determining the orientations and relative magnitudes (stress ratios) of the regional principal stress axes (see Angelier, 1994 for a review of the method). It is assumed that slip on the reactivated pre-existing planes of weaknesses and newly developed faults occur in accordance with the orientation and relative magnitudes of the principal stresses (Wallace, 1951; Bott, 1959). Moreover, a uniform stress ratio Φ is assumed for an area that is relatively small (not more than few tens of metres in dimension, see Hancock, 1985) compared to the regional stress field. However, this generalization is violated in a number of cases where a considerable amount of deviation of the computed shear stress and the observed slip direction occur in larger areas. The well known and modelled cases are as follows:

1. Presence of multiple phases of faulting especially with non-coaxial stress orientations and unequal magnitudes.
2. Interaction between major faults.
3. Fault terminations, especially a normal or reverse fault within a strike-slip fault system.
4. Large displacements along the faults, i.e. they accommodate larger strain and result in larger fault block rotations that increase the discrepancy between observed and calculated stress orientations, together with the relative stress magnitudes (Hardcastle and Hills, 1991; Pollard et al., 1993; Angelier, 1994; Toprak and Kaymakci, 1995; Homberg et al., 1997; Arlegui-Crespo and Simón Gómez, 1998; Twiss and Unruh, 1998; Kaymakci et al., 2003a,b; Alessio and Martel, 2004).
5. Triaxial strain conditions that produce faults having orthorhombic symmetry and the principal stresses are oblique with respect to earth surface. In such cases, the reduced stress tensor procedures produce more than one stress tensor configurations (Reches, 1978; Krantz, 1988; Nieto-Sameniego and Alaniz-Alvarez, 1997), as if there were two different deformation phases.

On the other hand, there is yet no method for determining the absolute magnitudes of past paleostresses. However, Bergerat (1987) and Angelier (1989) have proposed that paleostress magnitudes can be estimated by taking into consideration the vertical stress (σ_v) that is controlled by the thickness of the overburden (d), average density of the rock column (ρ) and acceleration due to gravity (g) using the equation;

$$\sigma_v = \rho \mathbf{dg}$$

The next step is the determination of which principal stress is the vertical stress. Using the standard paleostress inversion techniques such as the Direct Inversion Method (INVD of Angelier, 1990), maximum resolved shear stress and the stress ratios can be determined. Subsequently, from the calculated ratios and the vertical stress, absolute magnitudes of principal stress can be determined.

Since, the reduced stress tensor concept is based on the shape factor of the stress ellipsoid (Angelier, 1994), it is independent of absolute stress magnitudes and considers only the relative ratios of principal stress magnitudes. Therefore, it is independent of the pore-water pressure (σ_p) under hydrostatic conditions (i.e. pore-water pressure is smaller than minimum principal stress magnitude, $\sigma_p < \sigma_3$). In such cases, the only factor that affects the stress magnitude variations is the thickness of the overburden,with the other variables constant. Therefore, knowing the depth of faulting, the magnitudes of the principal stresses can be determined (Bergerat, 1987; Angelier, 1989).

Paleostress inversion studies involve the collection and analysis of fault-slip data wherever available in the field. Most of the time, there is very little information about the depth of faulting, since the determination of the amount of deposition and erosion requires very detailed information, necessitating a very careful examination of the rock column. In most continental areas such data has been eroded away and information about post-depositional changes such as the amount of compaction and density variations, water content, etc. has been lost.

This contribution, is aimed at presenting:

1. kinematic development of the Denizli Basin within the West Anatolian Horst Graben System (WAHGS, Western Turkey, Fig. 1) using major structures, fault slip data and recent travertine fissure occurrences collected in the field.
2. spatial distribution of stress ratios determined by using the reduced stress concept;
3. to discuss the possible causes of local stress magnitude variations in relation to above-mentioned constraints.

For this reason, first the stratigraphical, structural characteristics of the Denizli Basin will be presented, and then paleostress analysis will be presented and discussed.

2. Regional tectonics

The West Anatolian Horst-Graben System (WAHGS) extends from the Aegean Sea to central Anatolia (Fig. 1A) and it is one of the most rapidly deforming regions in the world (Dewey and Sengör, 1979; Le Pichon and Angelier, 1979; Alessio and Martel, 2004; Jackson and McKenzie, 1984; Eyidogan and Jackson, 1985; Sengör, 1987; Taymaz

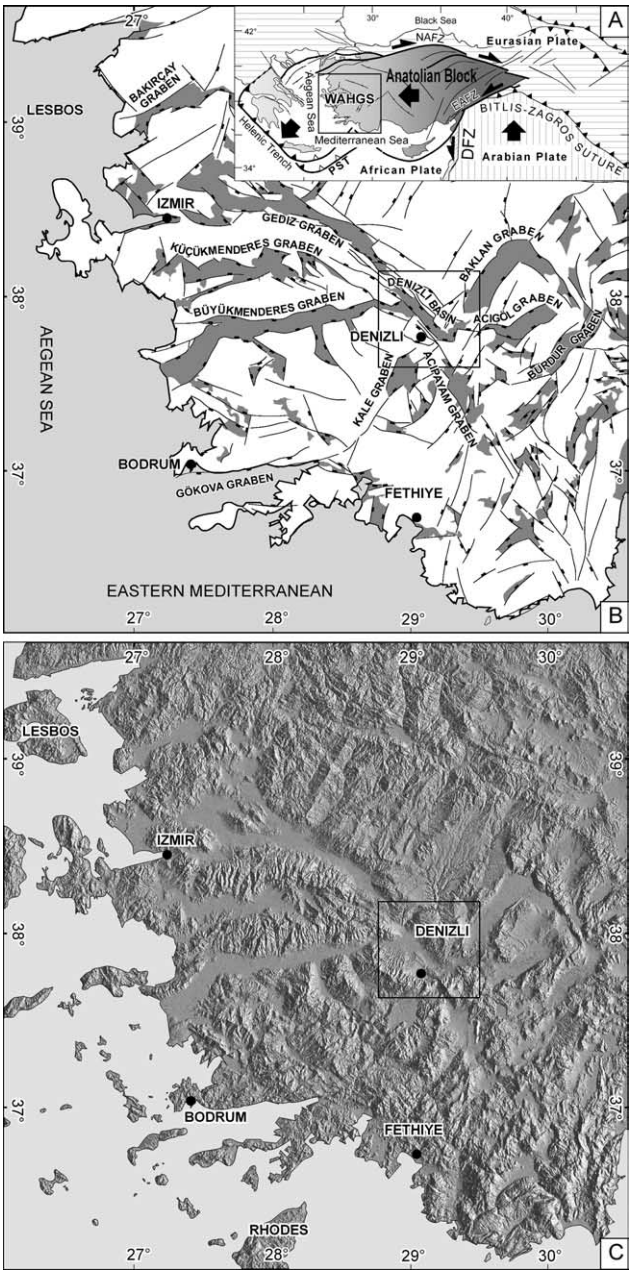

Fig. 1. (A) Tectonic outline of eastern Mediterranean area. DAFZ: Dead Sea Fault Zone, EAFZ: East Anatolian Fault Zone, NAFZ: North Anatolian Fault Zone, PST: Pliny-Strabo Trench. (B) Simplified map showing the major active basins in the western Anatolia. Box shows position of Denizli Graben. (C) Shuttle Radar Topographical Mission (SRTM) 3 arc seconds (~90 m) resolution shaded Digital Terrain Model of western Anatolia and eastern Aegean Sea.

et al., 1991; Taymaz and Price, 1992; Seyitoglu and Scott, 1991; Seyitoglu and Scott, 1996; Seyitoglu et al., 1992; Westaway, 1994; Straub et al., 1997; Lips, 1998; Walcott and White, 1998; Koçyigit et al., 1999; Reilinger et al., 1999; Bozkurt, 2000; Bozkurt, 2001; Bozkurt, 2003, Duermeijer et al., 2000; Gürer et al., 2003; Lips et al., 2001; McClusky et al., 2000; Reilinger and McClusky, 2001; Provost et al., 2003). It is characterized mainly by E–W trending major horsts and grabens, and NW–SE to NE–SW oriented relatively short and locally suspended cross-grabens (Bozkurt, 2003), contained within the major E–W trending horsts. The tectonic origin, age and structural development of these structures and direction of extension in the region are hot issues in the international literature. Four different models have been proposed for the origin and age of these structures, summarized in Bozkurt (2001) and Bozkurt (2003). Nevertheless, two different processes dominate in the Aegean region, including western Anatolia. These are the westward extrusion of the Anatolian Block and the N–S extension resulting from subduction of the Eastern Mediterranean crust below Greece, the Aegean Sea and Turkey. Roughly, the North Anatolian Fault Zone (NAFZ) forms the northern boundary of the extensional area, whereas the southern boundary is rather diffuse and may reach as far south as the Crete-Rhodes depression and the Hellenic and Pliny-Strabo trenches (Glover and Robertson, 1998; Kokkalas and Doutsos, 2001; Ten Veen and Kleinspehn, 2003) (Fig. 1).

The major, roughly E–W trending basins in the WAHGS from north to south are Bakırçay, Gediz, Küçükmenderes, Büyükmenderes and Gökova grabens (Fig. 1B). These basins are very well defined by horst-graben morphology that may reach up to 200 km in length, where the main peaks of the horsts may reach up to 2 km in height, while the graben floors lie at about sea level (Fig. 1C). The Denizli Graben is situated in an area where three major E–W grabens approach at their eastern ends. Thus, it forms the eastern continuation of the Büyükmenderes Graben and is separated from the Gediz Graben by a topographic high, about 10 km long, around Buldan (Figs. 1 and 2A) and from the Küçükmenderes Graben by a high about 40 km long, although some of the basin-bounding faults are shared by these grabens, such as the Buldan and Buharkent faults which traverse both basins (Fig. 2A).

The Denizli Basin as a whole is bounded in the north by the Çökelezdag Horst and in the south by the Babadag and Honazdag Horsts (Fig. 2). In the central part, it is traversed by one of the faults of the Laodikia Fault Zone that also controls the northern margin of the Acipayam Graben. It is a NW–SW elongated basin approximately 50 km long and 25 km wide, and comprises two Quaternary sub-basins, namely the Çürüksu Graben in the north and the Laodikia Graben in the south, separated by a large basin-parallel topographical high along which Late Miocene–Pliocene fluvio-lacustrine deposits are exposed (Fig. 2). The Çürüksu graben is controlled in the north by the Pamukkale Fault Zone and in the south by the Laodikia Fault Zone. The Laodikia Graben is controlled by one of the branches of Laodikia Fault Zone in the north and Babadag Fault in the south. To the east of Denizli town center, north of Honaz and around Kaklık, the Denizli Basin has a staircase geometry delimited in the south by the Honaz and Kaklık Faults, around which the main boundary faults of the NE–SW trending Baklan and Acipayam grabens interfere (Fig. 2).

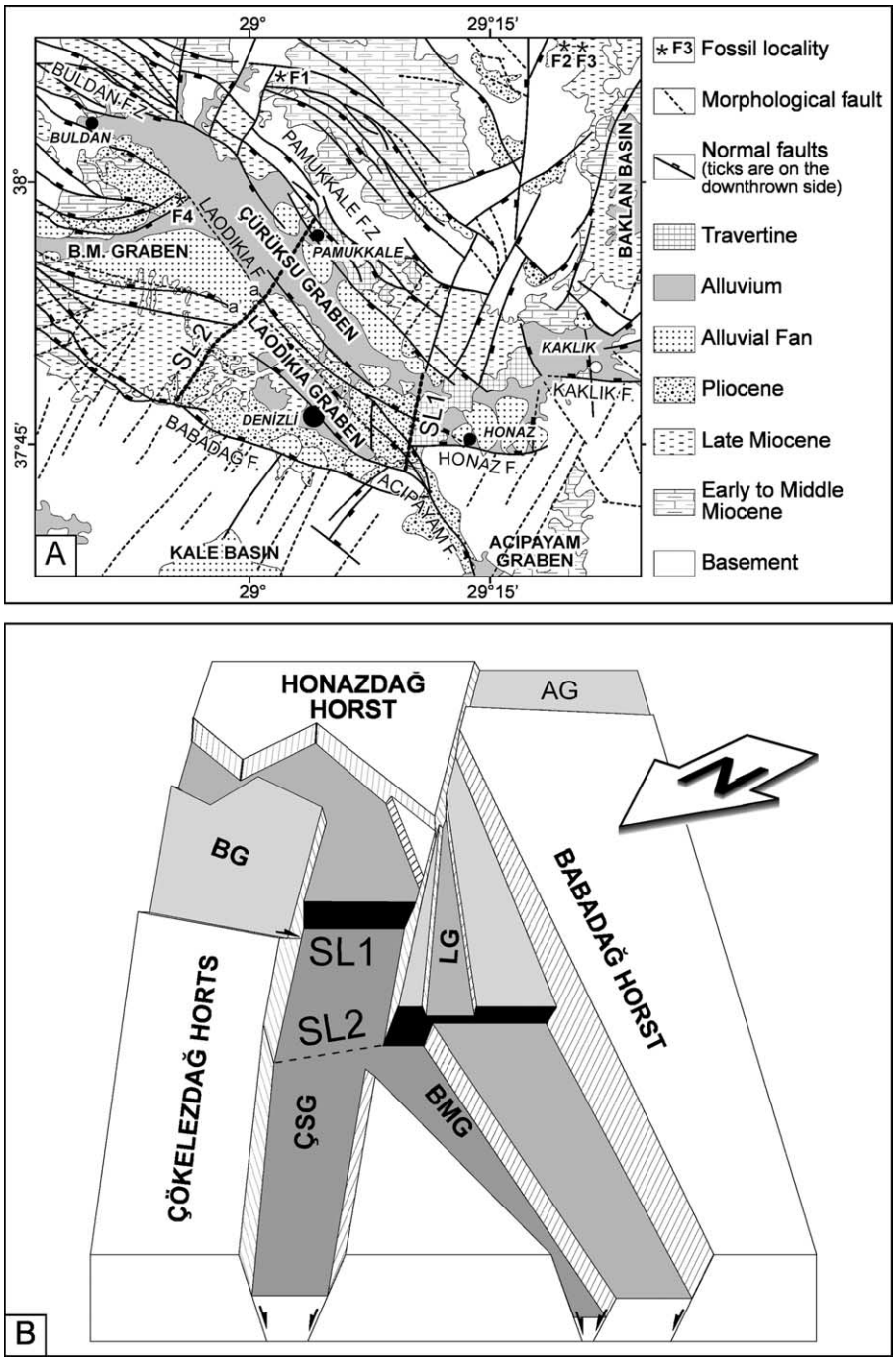

Fig. 2. (A) Geological map of Denizli Basin prepared from 500,000 scale Geological Map of Turkey (General Directorate of Mineral Research and Exploration-MTA, Ankara/Turkey), Landsat ETM+ image and SRTM data. a–a′: 1.5 km displacement along SL2, B.M. Graben: Büyükmenderes Graben, F1–F4: fossil localities, F.Z.: Fault Zone,.SL1 and SL2: subsurface structures. Numbers around the map are UTM coordinates (Zone 35, Map Datum: WGS84). (B) simplified block diagram of the Denizli Basin. Basin infill is not drawn. AG: Acıpayam Graben, BG: Büyükmenderes Graben, ÇSG: Çürüksu Graben, LG: Laodikia Graben.

3. Stratigraphy and age of the basin infill

The infill of the Denizli Graben rests on various metamorphic assemblages including marbles and some schists (Figs. 2 and 3). These metamorphic units are thought to related to collision and obduction processes that took place after the closure of Neotethys Ocean in the Late Cretaceous to Oligocene interval (Sengör and Yilmaz, 1981; Bozkurt and Park, 1994). These metamorphic units constitute the basement to the infill of the Denizli Basin. The infill comprises three different assemblages and Recent alluvial units and travertine occurrences (Fig. 3). The ages

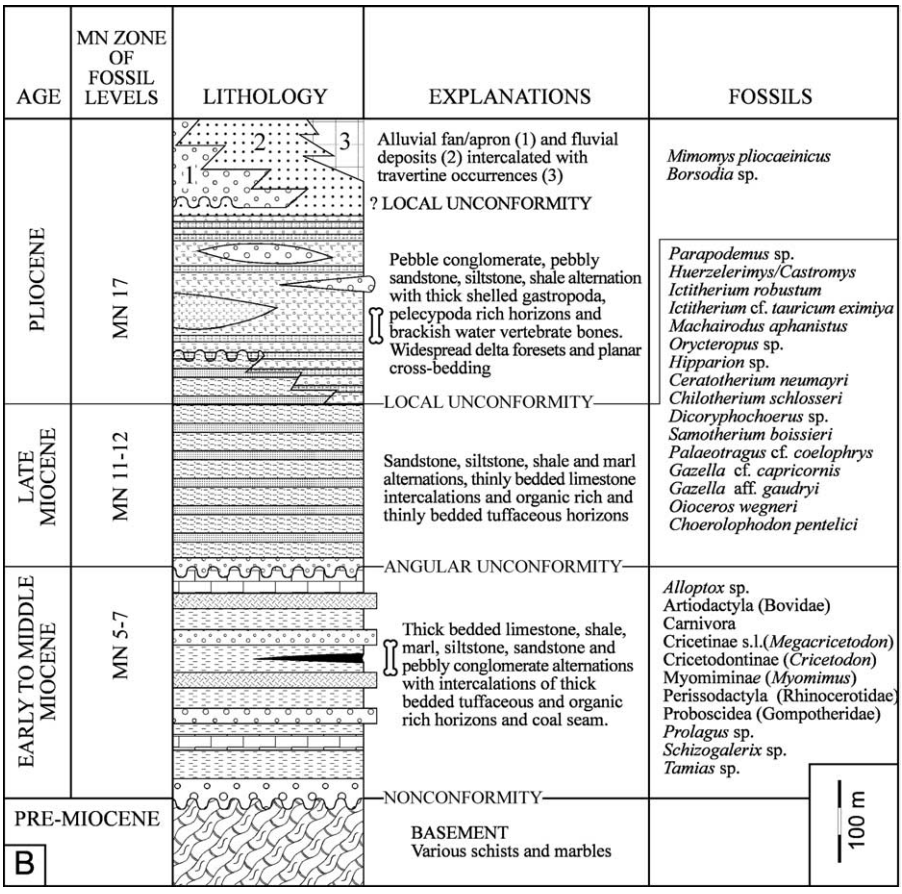

Fig. 3. Generalized stratigraphical columnar section of the Denizli Basin. Bone symbol indicates fossil levels.

of these assemblages are based on Saraç et al. (2001). A vertebrate fauna collected from various localities (F1–F4 in Fig. 2A) in the basin were identified by Hans De Bruijn (2002, personal communication, Utrecht University, the Netherlands).

3.1. Early to Middle Miocene units

These are the oldest infill of the Denizli Basin and comprise alternations of thickly bedded limestone, shale, marl, various tuffaceous horizons, siltstones, sandstones and lenses of conglomerates resting on the basement units (Fig. 3). This assemblage also includes various organic rich horizons and a coal seam in the north of Pamukkale around F1 (Fig. 2A). This unit is exposed mainly in the northern part of the Denizli Basin and extends further north, beyond the present configuration of the basin, which implies that it was deposited before the Denizli Basin acquired its present geometry. On the northern margin of the basin, it includes a series of small scale NE–SW trending open to closed anticlines and synclines oblique to basin-bounding faults. In the samples collected from middle parts of the unit, the following vertebrate fossils were identified: *Alloptox* sp., Artiodactyla (Bovidae), Carnivora, Cricetinae s.l. (*Megacricetodon*), Cricetodontinae (*Cricetodon*), Myomimina (*Myomimus*), Prissodactyla (Rhinocerotidae), Proboscidea (Gompotheridae), *Prolagus* sp., *Schizogalerix* sp., *Tamias* sp. These fossils characterize European mammal zone MN 5–7. Based on this fossil assemblage an Early to Middle Miocene age is assigned to the oldest assemblage of the Denizli Basin.

3.2. Late Miocene units

This assemblage is exposed mainly in the central part of the Denizli Basin, along a topographical high between the Laodikia and Çürüksu grabens, and in the eastern part of the Denizli Basin, where it is intersected by the Baklan Graben. It comprises rhythmic alternations of sandstone, siltstone, shale and marl, thinly bedded limestone intercalations and organic rich and thinly bedded tuffaceous horizons (Fig. 3). Planar cross-bedding and graded bedding is very common in the sandstone and pebble conglomerates, implying that these horizons were deposited by turbidity currents. A number of layers with accretions of thick-shelled pelecypoda and gastropoda imply brackish water conditions for the assemblage. It is characterized also by a series of NW–SE trending open anticlines and

synclines roughly parallel to the long axis of the basin. No fossils were found within the Denizli Graben. However, from two different localities (F2 and F3 in Fig. 2A) in the southern part of the Baklan Graben the following vertebrate fauna were identified: *Parapodemus* sp., *Huerzelerimus/Castromys, Ictitherium robustum, Ictitherium* cf. *tauricum eximiya, Machairodus aphanistus, Oryctropus* sp., *Hipparion* sp., *Ceratotherium neumayri, Chilotherium schlosseri, Dicoryphochoerus* sp., *Samotherium boissieri, Palaeotragus* cf. *coelophrys, Gazella* cf. *capricornis, Gazella* aff. *gaudryi, Oioceros wegneri, Choerolophodon pentelici.* These fossils characterize European MN 11–12 mammal zones. Based on this fauna a Late Miocene age is assigned to the assemblage.

3.3. Pliocene units

This assemblage is exposed mainly in the western and SE part of the Denizli Graben. It is characterized by alternations of a very thick pebble conglomerate, pebbly sandstone, siltstone, shale with thick shelled gastropoda, pelecypoda rich horizons and bones of brackish water vertebrates, possibly hippopotamus (personal communication, Hans de Bruijn) (Fig. 3). Planar cross-bedding, delta foreset bedding, scour and fill structures are very common in the assemblage. Cross-beds and pebble imbrications measured in few localities implies SW to NE direction of sediment transport from the Babadag Horst towards the basin center. Towards the southern margin of the Denizli Graben the bottom of the unit rests on the Late Miocene, above an erosion surface, while in the central part of the basin it grades into a Late Miocene assemblage and in the samples collected from fossil locality F4 (Fig. 2A) *Mimomys pliocaeinicus, Borsodia* sp. were identified, which characterize European mammal zone MN 17. Therefore, a Pliocene age is assigned to this assemblage.

Very thick planar cross-bedded conglomerates rich in pelecypoda and gastropoda shells, a local unconformity at the margin and a gradational contact in the central part, indicate that this unit and the upper part of the Late Miocene assemblage was deposited within a tectonically active environment in which sediments were shed mainly from the southern margin of the basin, possibly from the Babadag and Honaz Horsts.

3.4. Alluvial and travertine occurrences

Alluvial deposits in the Denizli Basin are developed mainly in the Çürüksu and Laodikia grabens and along the active faults bordering the actively developing basin margins. A linear arrangement of alluvial fans and seismic activity are evidence that these faults are currently active. The alluvial fans may reach up to 3 km length and 5 km width along the northern margin of the graben, and can be easily identified on satellite images. They are composed mainly of loose conglomerates and sandstones. Along the Laodikia Fault, the alluvial fans are dominated by sandstones and fine clastics as they shed detritus from Late Miocene units.

Travertine occurrences are concentrated mainly along the northern and eastern margins of the basin (Fig. 2A). Ancient Hieropolis (Pamukkale), which is included in the *World Heritage List* is located on the northern margin of the basin where travertine is still being deposited from thermal springs (Hancock and Altunel, 1997; Hancock et al., 1999). In some localities the discharge of the springs has been artificially increased by drilling, which may reach to depths of 60–80 m, indicating that the hot water aquifers are very shallow. Based on U-series dating, some of the travertine is as old as 400,000 years. It is calculated that fissures in the travertine are opening at a rate of 1.5–3 mm/year (Altunel and Hancock, 1993).

4. Paleostress

Approximately 530 fault-slip data were collected from 42 locations, together with extension veins, travertine fissure orientation data (Fig. 4) and conjugate faults that did not have striations on the fault surfaces. In nine of these locations, overprinting slickensides were noted. The data were processed using the Direct Inversion Method (INVD) of Angelier (1990). In the analysis and processing of the data, the methodology outlined in Kaymakci (2000) and Kaymakci et al. (2000) was used. During the inversion process, as well as field-based separations, automatic separation processes (Angelier and Manoussis, 1980; Hardcastle and Hills, 1991) were also applied, to test whether the data belong to single or multiple phases of faulting. In the analysis the allowable maximum misfit angle (ANG) was taken as 15° and maximum quality estimator value (RUP) was taken as 45°. It was observed that most of the data for each site was consistent; this was also valid for the overprinting slickensides which were processed separately. In addition, faults which exceeded these values were separated and analyzed separately. They make up less than 1% of the total data, indicating that the collected data for each set belong to single event, with almost no mixed data. From the fault-slip data 50 stress configurations were constructed. Among these, 28 yielded an approximately NE–SW direction of extension (Fig. 4A), 17 of them yielded a NW–SE extension (Fig. 4B) and two of them yielded an E–W direction of extension; these were not included in the analysis because there are only 4 measurements of slip data, which is not statistically valid (see Table 1).

4.1. Stress trajectories

Using the constructed paleostress orientations for the NE–SW and NW–SE extension directions smoothed trajectories were constructed manually for the σ_2 and σ_3 (Fig. 5) since σ_1 is generally vertical. Since the deviation of

the stress orientations is gradual, especially for the NE–SW extension directions, manual plotting was thought to be adequate in drawing the trajectories, although various computerized interpolation techniques may be used (e.g. Lee and Angelier, 1994). As the principal stress trajectories are always perpendicular to each other in 3D (Treagus and Lisle, 1997), but the horizontal components may not be perpendicular to each other, for such cases, the

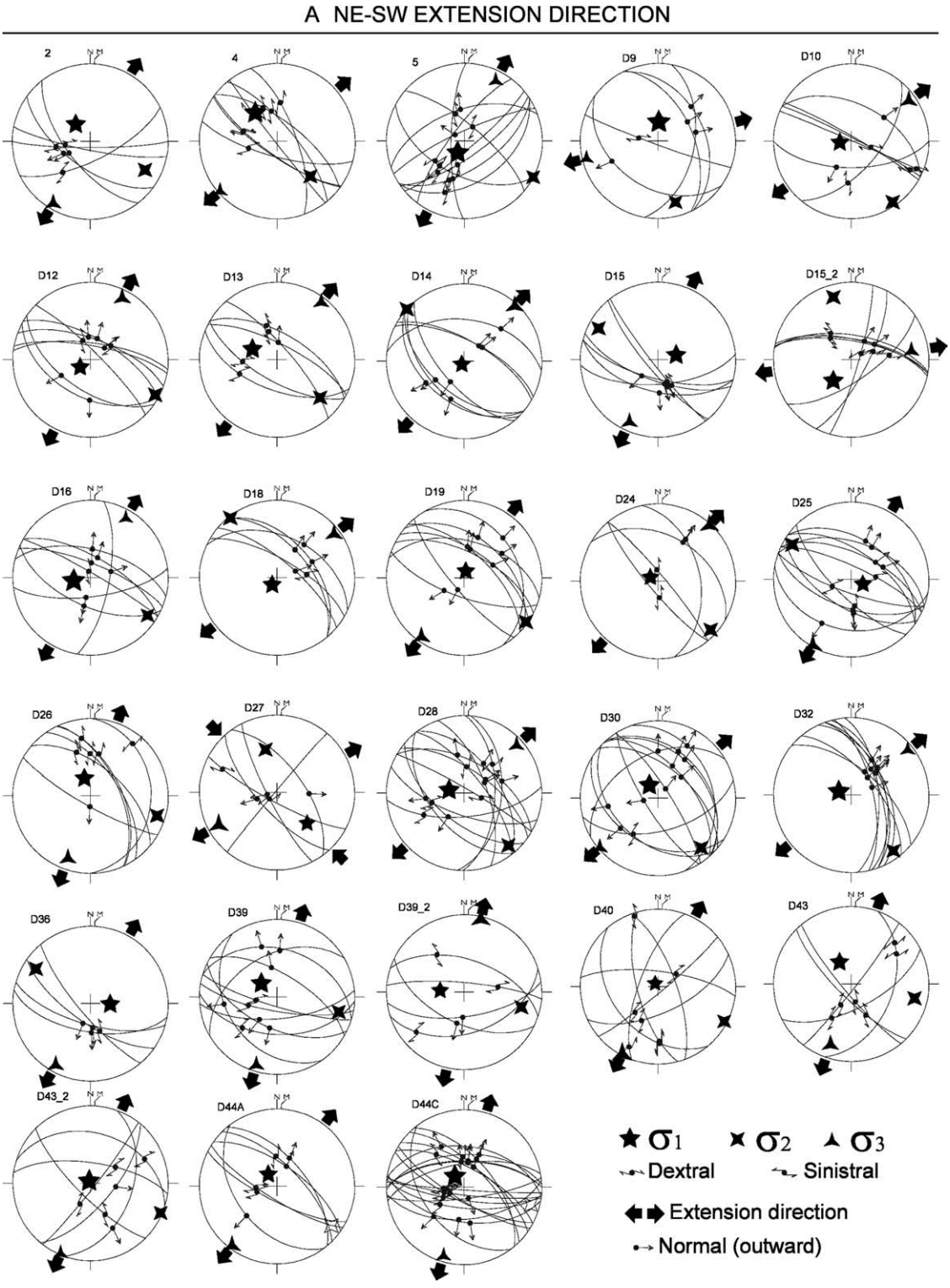

Fig. 4. (A–B) Cyclographical traces, stress orientations and striations on the faults (Lower hemisphere Equal area projection) for the (A) NE–SW and (B) NW–SE extension directions. (C) simplified map of travertine fissure near Pamukkale (see Fig. 2 for its location) and rose diagram travertine fissure orientations collected from all travertine occurrences in the Denizli Basin. Determinations are in Table 1.

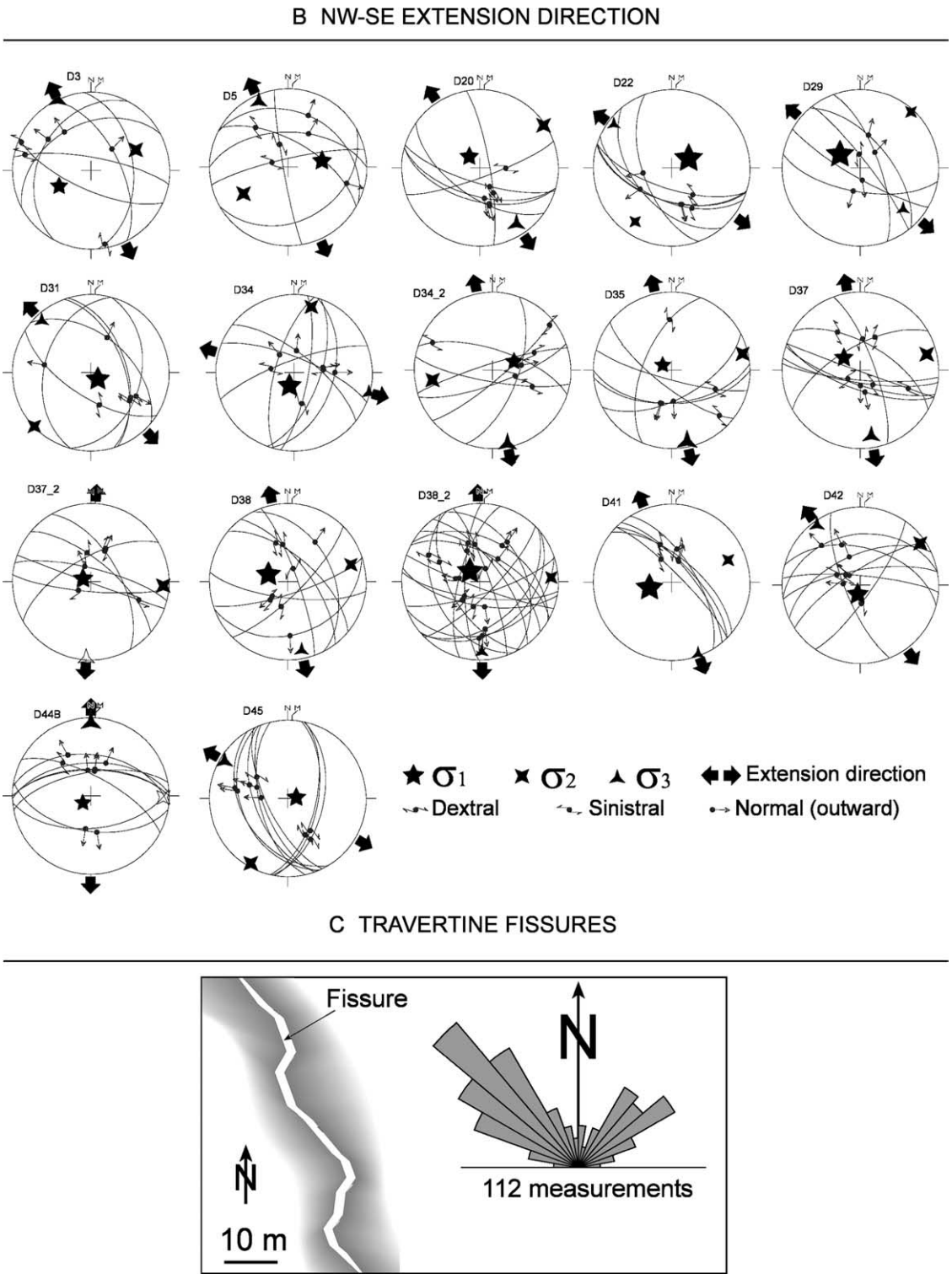

Fig. 4 (*continued*)

horizontal component of the σ_3 directions were taken as the reference, and the σ_2 direction were adjusted accordingly. It is important to note that, the constructed trajectories should be regarded as qualitative rather than definitive (see Ramsay and Lisle, 2000).

4.2. Plotting stress ratios

It is assumed that in the brittle upper crust the development of fractures and faults obeys the Coulomb–Mohr criterion. This states that yield occurs along the most

Table 1
Detailed information about the stress tensors in the Denizli Basin

Site	x	y	σ_1 (D/P)		Φ_1	σ_2 (D/P)	Φ_2		σ_3 (D/P)		Φ_3	Φ	#	RUP	ANG
NE–SW extension															
1	689194	4182255	320	66	0.90	117	22	−0.07	211	8	−0.83	0.44	5	26	7
3	694709	4178602	323	52	0.95	137	38	−0.21	229	3	−0.74	0.31	7	31	12
5	694172	4180307	210	76	0.96	118	1	−0.25	28	14	−0.72	0.28	11	32	11
6	683420	4202611	3	70	0.97	164	19	−0.28	256	6	−0.69	0.24	5	26	6
7	667443	4207304	264	78	0.86	146	6	0.02	55	10	−0.87	0.52	6	18	11
8	687936	4184230	235	77	0.87	118	6	−0.01	27	12	−0.86	0.50	7	27	9
9	685683	4186637	294	62	0.91	131	27	−0.10	38	7	−0.81	0.41	5	33	5
10	686471	4187644	219	86	0.83	312	1	0.07	42	4	−0.90	0.56	7	24	10
11A	689096	4186726	75	70	0.91	298	15	−0.10	205	13	−0.81	0.42	6	22	7
12	690712	4185518	260	72	0.97	123	13	−0.29	31	12	−0.68	0.24	7	35	12
13	685252	4186949	216	81	0.87	322	3	0.00	52	8	−0.87	0.50	5	17	6
14	683545	4189364	13	83	0.84	126	3	0.04	216	7	−0.89	0.54	8	27	9
17	667620	4198901	298	81	0.81	133	9	0.11	42	2	−0.92	0.60	4	40	10
18	667362	4196041	111	77	0.82	301	13	0.09	210	2	−0.91	0.58	10	31	10
19A	676025	4189479	341	70	0.89	107	12	−0.05	200	16	−0.84	0.46	7	32	9
20	674474	4188787	136	44	0.76	345	42	0.18	241	15	−0.94	0.66	5	45	13
21A	672643	4188203	282	74	0.93	140	13	−0.14	48	10	−0.78	0.37	12	30	10
21B	672643	4188203	2	71	0.89	100	3	−0.05	191	19	−0.84	0.46	5	30	9
23	674689	4191464	327	73	0.93	139	16	−0.16	230	2	−0.78	0.36	11	28	9
25	672864	4186374	287	76	0.95	143	11	−0.21	51	8	−0.74	0.32	8	12	5
28	709851	4193922	91	69	0.89	303	18	−0.06	209	10	−0.84	0.45	4	19	2
31A	692589	4195347	311	68	0.93	104	20	−0.15	197	9	−0.78	0.37	9	28	9
31B	692589	4195347	274	65	0.79	105	25	0.14	13	4	−0.93	0.62	5	43	15
32	686924	4198729	319	85	0.69	118	4	0.28	208	2	−0.97	0.76	7	45	15
35A	694689	4177174	332	64	0.87	103	18	−0.02	199	19	−0.86	0.49	6	42	10
35B	694689	4177174	331	87	0.96	113	2	−0.24	203	2	−0.72	0.29	6	45	12
36	691221	4180497	320	75	0.96	105	12	−0.23	197	8	−0.73	0.29	19	41	14
36B	691221	4180497	230	79	0.73	91	8	0.23	0	7	−0.96	0.71	8	23	7
NW–SE extension															
2	694373	4179060	244	53	0.81	65	37	0.11	335	1	−0.91	0.59	5	32	10
4	694172	4180307	79	54	0.89	240	34	−0.05	336	9	−0.84	0.46	6	29	13
15	685082	4190849	317	74	0.86	56	3	0.00	147	16	−0.87	0.50	6	41	11
16	685028	4191964	61	70	1.00	214	18	−0.49	307	8	−0.51	0.01	6	21	7
22	674728	4191893	304	64	1.00	42	4	−0.47	134	25	−0.53	0.03	5	40	13
24	672405	4187425	131	80	0.98	227	1	−0.30	317	10	−0.67	0.23	6	32	11
26A	712513	4192252	200	76	0.98	15	14	−0.30	105	1	−0.67	0.23	7	34	13
26B	712513	4192252	67	66	0.79	261	24	0.13	169	5	−0.92	0.62	6	34	14
27	711842	4192846	301	79	0.72	77	8	0.24	168	7	−0.96	0.71	4	28	12
29A	701113	4188263	308	68	0.87	76	14	0.00	171	16	−0.86	0.50	8	43	14
29B	701113	4188263	292	81	0.90	93	8	−0.06	184	3	−0.83	0.45	6	45	13
30A	693536	4190926	291	68	0.99	75	18	−0.35	169	12	−0.63	0.17	8	32	8
30B	693536	4190926	317	75	1.00	87	10	−0.41	179	12	−0.58	0.11	18	42	15
33	686316	4177532	257	66	1.00	68	24	−0.45	160	3	−0.55	0.06	5	23	9

(*continued on next page*)

Table 1 (*continued*)

Site	x	y	σ_1 (D/P)		Φ_1	σ_2 (D/P)	Φ_2		σ_3 (D/P)		Φ_3	Φ	#	RUP	ANG
34A	691928	4178329	196	80	0.94	55	8	−0.19	324	6	−0.76	0.33	8	42	13
37	679913	4187331	83	81	0.87	210	5	−0.01	301	7	−0.86	0.49	9	34	11
E–W extension															
11B	689096	4186726	220	61	0.92	344	17	−0.12	82	23	0.86	0.39	4	45	13
19B	676025	4189479	245	67	1.00	351	7	−0.48	84	22	−0.52	0.02	4	35	13

X,*Y*, UTM co-ordinates (zone 35S); Φ_1, Φ_2, Φ_3, magnitude ratios of principal stresses; D/P, direction plunge; Φ, stress ratio; #, number of faults per site; RUP, maximum allowed quality value; ANG, maximum allowed angular divergence.

favorable plane of weakness, when the maximum shear stress along the plane exceeds its strength (Jaeger and Cook, 1969). For dry conditions this relationship is given by $\tau_{max} = \tau_c + \mu s_n$ where τ_{max} is maximum shear stress, τ_c is cohesion, μ is the coefficient of friction and σ_n is the normal stress along the plane. Where rocks contain pore-water, effective stress should be taken into consideration and pore-water pressure should be subtracted from the normal stress. In natural cases, rockmass strength, pore-water conditions and variations in time cannot be determined, complicating the determination of absolute stress magnitudes. As mentioned previously, relative stress magnitudes, calculated by the direct inversion method, are the manifestation of absolute stress magnitudes, which can be calculated easily, if the depth of faulting and vertical stress is known. For that reason, the σ_3 ratio (Φ_3) which is the relative magnitude of minor stress and the stress ratio (Φ) are plotted for the Denizli Basin in order to establish the spatial variation of stress ratios. In this respect, the ratios of σ_1, σ_2, and $\sigma\Phi_3$ (Φ_1, Φ_2, Φ_3 respectively) are considered as the relative stress magnitudes. In plotting the stress ratios, three variables were used (*X*,*Y*,*Z*) where the first two variables define the geographical position and third variable is the relative magnitude or ratio. The relative magnitude values and stress ratio (Φ) are obtained during the construction of paleostress configurations using Angelier's (1988) software. Then, linear interpolation with triangulation technique is applied (Davis, 2002) to estimate the spatial variation of the relative stress magnitudes and stress ratios (Fig. 6). The plots obtained were overlain onto a structural map of the Denizli Basin in order to evaluate the relationships between the stress distribution and the structure (Fig. 6A–C). Since there are no data from the Quaternary alluvium being deposited in the Çürüksu Graben sampling stations are clustered mainly in the southern part of the Denizli Basin around the Laodikia Graben, and north of the Çürüksu Graben, along the Pamukkale Fault Zone (Fig. 5A). Such clustering and gaps in the alluvial data might produce statistical artifacts. In order to overcome this problem, the data cluster in the southern part of the area is treated separately (Fig. 6D and E).

5. Discussion

5.1. Tectonic phases versus stress permutations

One of the most important issues in paleostress inversion studies is to date the constructed stress configurations. This may be achieved by dating the stratigraphical horizons involved in the faulting and the relationship between sedimentation and tectonics (Angelier, 1994). In this respect, syn-sedimentary structures provide invaluable information for the dating of constructed stress configurations.

Most of the data from the Denizli Basin were collected from Late Miocene to Pliocene and younger units (Quaternary travertines). In some localities, growth

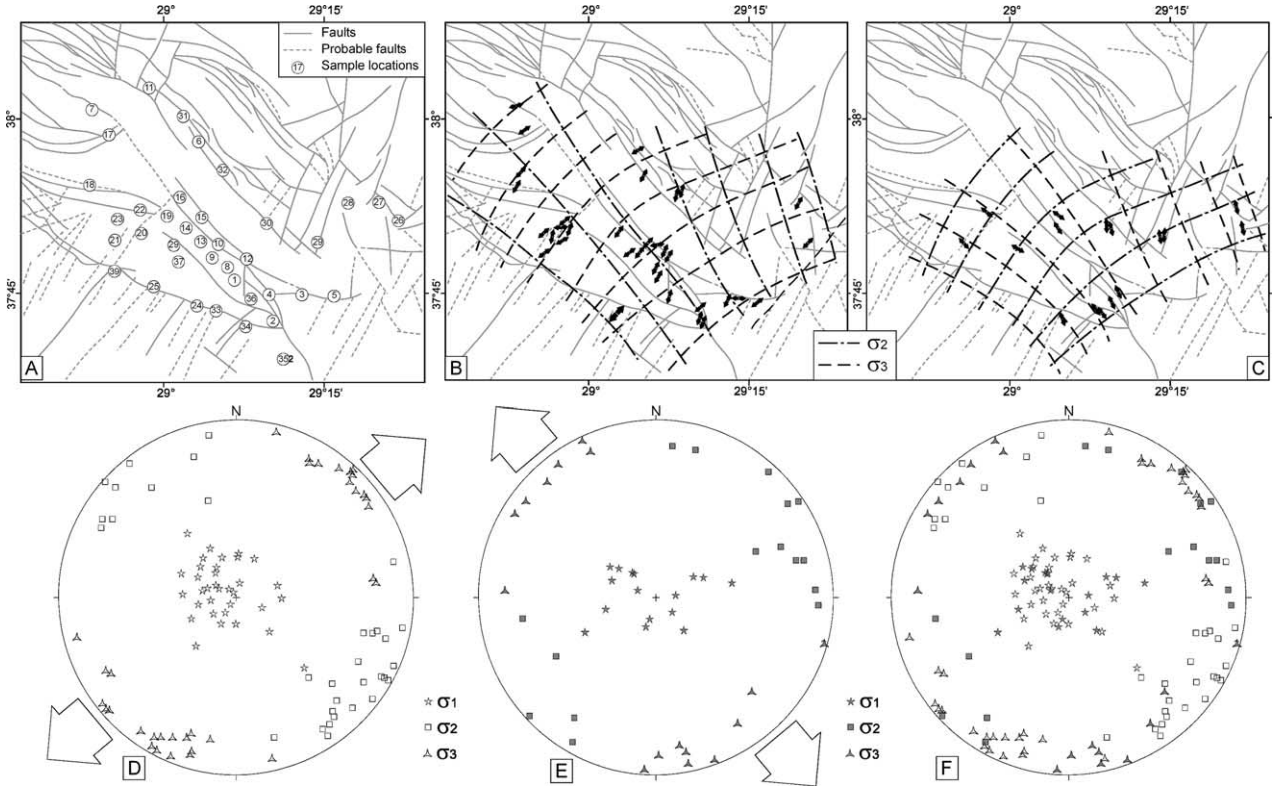

Fig. 5. (A) Structural map and sampling sites. Orientation of σ_3 directions (arrows) and smoothed trajectories of horizontal components of σ_2 and σ_3 for the (B) NE–SW and (C) NW–SE extension directions. (D–E) Lower hemisphere, equal area projection of paleostress orientations for both the NE–SW and NW–SE extension directions, respectively. (F–D) and (E) a shown on the same plot. Note that sσ_2 and σ_3 for different sets almost overlap.

faults were encountered during field studies (Fig. 7). In these localities, the growth faults were developed within the Late Miocene units and display typical thickening on the down-thrown side and thinning on the up-thrown side. Similar relationships were also observed within the Pliocene units (Fig. 7B). Paleostress inversion studies in such localities yielded consistent results in both Late Miocene and Pliocene units. On the other hand, travertine fissures measured in the field indicate both NE–SW and NW–SE directions of extension (Fig. 4C, see also Altunel and Hancock, 1993). Therefore, it is concluded that the NE–SW and NW–SE directions of extension were both operative from the Late Miocene to Recent. A question then arises concerning the order of development of these extension directions. Active faults that determine the present configuration of the Denizli Basin trend NW–SE and have a very strong dip-slip component. In addition, the long axes of fissures in Recent travertine occurrences are also oriented NW–SE, parallel to the basin-bounding faults. This suggests that the presently active extension direction is NE–SW. It can therefore be concluded that the NW–SE phase of extension predated the NE–SW extension phase. However, the long axes and the basin-bounding faults of the basins to the east of the Denizli Basin, including the Baklan, Acıgöl and Burdur basins, are oriented NE–SW and recent earthquakes in this area indicate local NW–SE extension directions (Taymaz and Price, 1992). In addition, it is observed that σ_1 directions for both NE–SW and NW–SE extension directions overlap when σ_2 and σ_3 are interchanged (Fig. 5F). These facts indicate that both the NE–SW and NW–SE extension directions are presently active and that they may frequently interchange in time and place. This relationship is due to stress permutations between σ_2 and σ_3, possible when magnitudes of σ_2 and σ_3 are very close, but not equal, to each other (Homberg et al., 1997). A similar pattern is also possible under conditions of triaxial strain (Donath, 1962; Reches, 1978; Krantz, 1988; Arlegui-Crespo and Simón-Gómez, 1997; Nieto-Samaniego and Alaniz-Alvarez, 1997) under which four sets of faults displaying orthorhombic symmetry may be developed (Reches, 1978). Since most of the σ_1 directions are sub-vertical, other stresses are sub-horizontal and the structures are almost perpendicular to each other, stress permutation rather than triaxial strain is most likely to occur in this situation. Whatever the mechanism responsible for the two directions of extension, it can be concluded that only one stress regime has occurred in the Denizli Basin since the Late Miocene. This conclusion does not rule out the possibility of multiple coaxial stress phases, which is a very difficult problem to resolve.

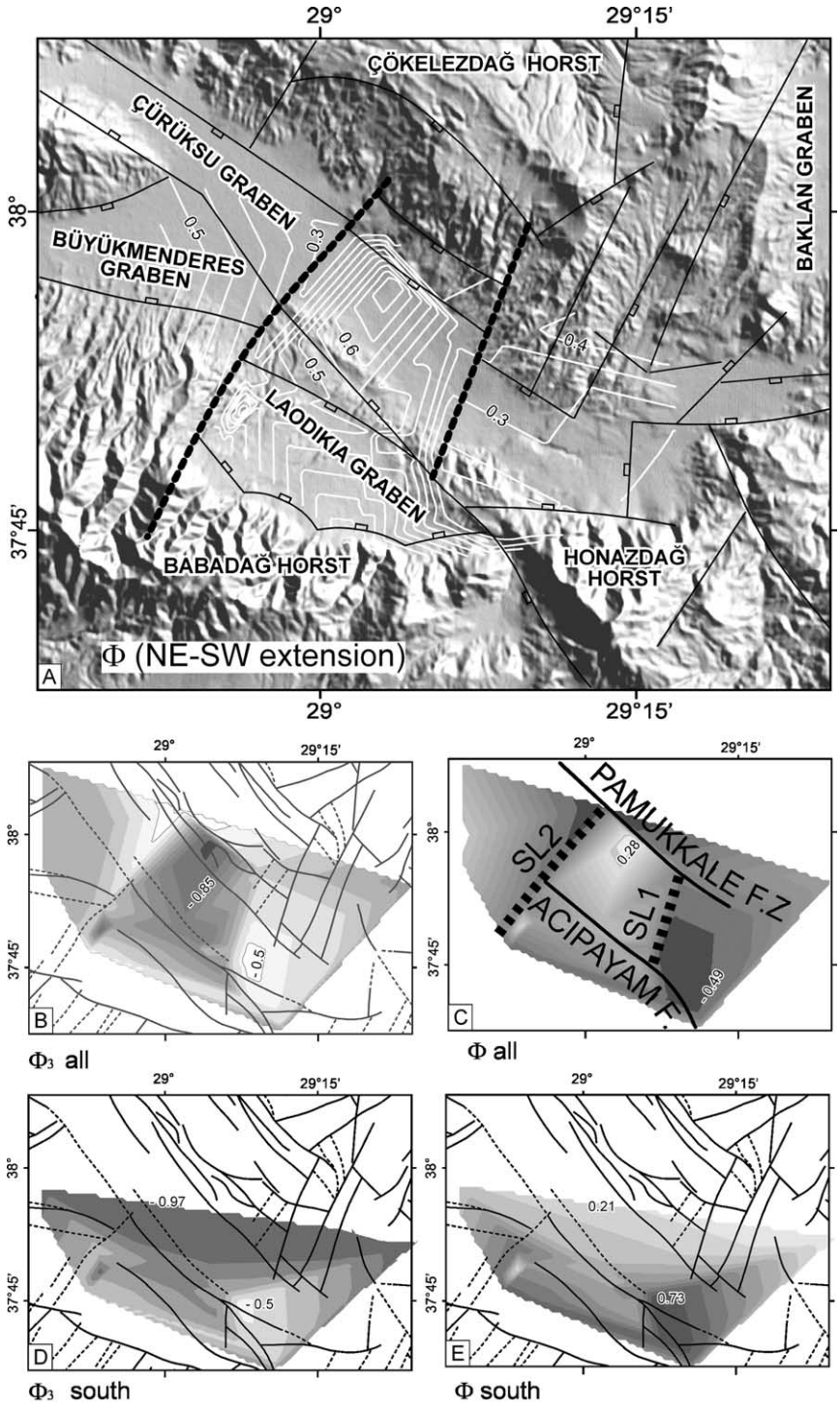

Fig. 6. (A) Distribution of relative stress magnitude ratios (Φ), for the NE–SW extension direction, overlaid onto shaded relief image of SRTM data and major structures around the Denizli Basin. Numbers indicate contour values. (B–C) Distribution of relative stress magnitudes for the σ_3 (Φ_3) and stress ratio (Φ) for whole data, and (E–F) for the southern part of the Denizli Basin. Distributions curves are prepared using the 'triangulation with linear interpolation' technique (Davis, 2002). SL1–SL2: subsurface structures/lineaments. Numbers (in B–F) indicate minimum and maximum values of the contours.

5.2. Distribution of relative stress magnitudes

Plots of both the σ_3 magnitude ratio (Φ_3) and the stress ratio show sharp changes across two axes (SL1 and SL2, Figs. 2B, 6C). These axes also correspond to a sharp change in basin geometry and in the trends of the major faults which determine the active configuration of the basin. Similar configurations are observed in the whole data set and also for the southern clusters. As may be seen seen in Fig. 6 there are very prominent deflections in the

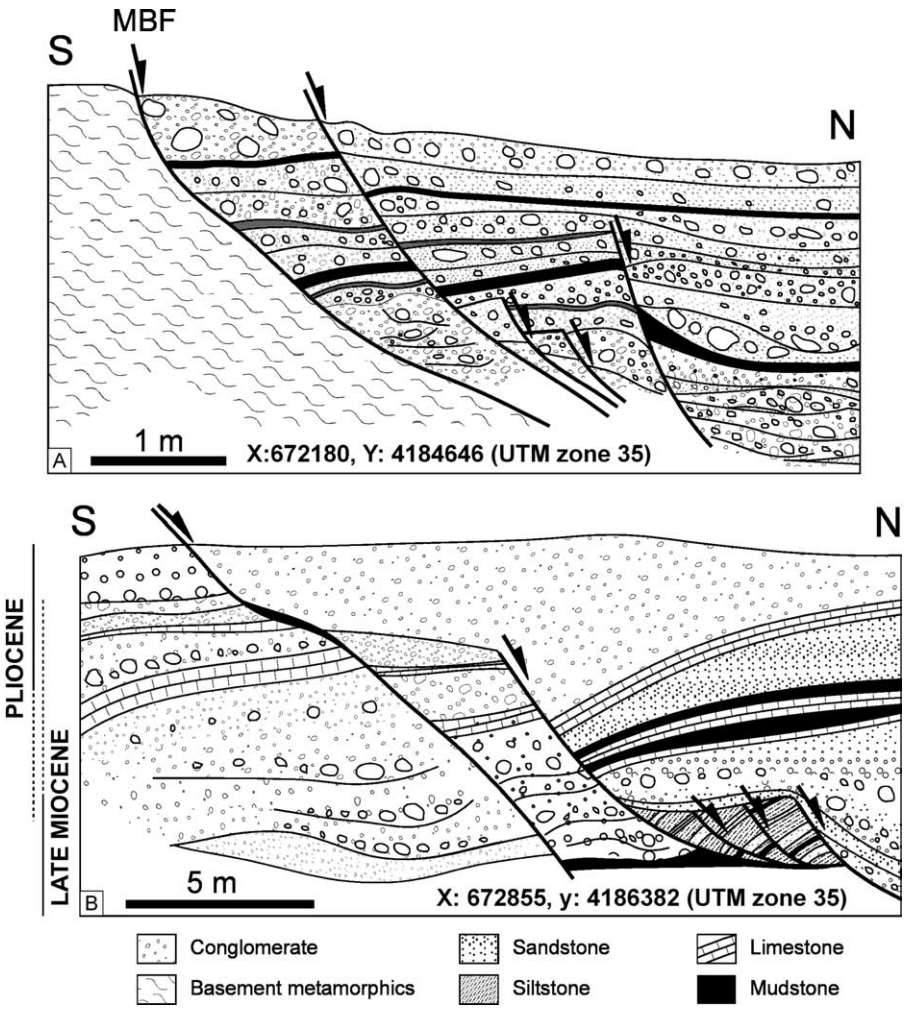

Fig. 7. Field sketches of growth faults observed in the (A) Late Miocene and (B) Late Miocene to Pliocene units between the sites 12–16. MBF: Main Boundary Fault. All levels are very rich in thick shelled brackish water gastropoda and pelecypoda.

stress magnitudes along SL1 and SL2. In addition, the bounding faults are oriented approximately E–W to the east of SL1, but to the west are oriented NW–SE. Along SL2, Late Miocene to Pliocene units are separated sinistrally by about 1.5 km (a–a' in Fig. 2A). In addition, to the west of this line the active graben floor of the Çürüksu Graben becomes enlarged in a N–S direction towards the Büyükmenderes Graben (Fig. 2B). These observations suggest that SL1 and SL2 in the Denizli Basin are subsurface structures which separate areas with different major stress magnitudes. It is proposed that SL1 results from the intersection of Denizli Basin with the Baklan Graben, where stress permutations are amplified due to the interference of the NW–SE extending Baklan Basin (Taymaz and Price, 1992) with the dominantly NE–SW extending Denizli Basin. This is indicated by very low stress values to the east of SL1 (Fig. 6A); the lowest values are obtained near the Honaz Fault and in the central part of the Pamukkale Fault Zone.

A similar mechanism may also be proposed for the origin of SL2. It is located where the Büyükmenders Graben is intersected by the Denizli Graben (Fig. 2). In addition, most of the travertine occurrences are located in the northern part of the Denizli Basin and to the east of SL2 (Fig. 2A). The travertines originate from thermal springs that are located along the faults in the Pamukkale Fault Zone, as well as in the alluvial plain of the Çürüksu Graben. Wells drilled in the basin by local people and the General Directorate of Mineral Research and Exploration (MTA-Ankara/Turkey), indicate that the hot water reservoir is a confined aquifer under pressure, confirmed by the occurrence of artesian wells. The local stress regime is different to the east and west of the SL2, as indicated in Fig. 6.

Using the information given above it is concluded that plotting the distribution of local relative (reduced) stress magnitudes and stress ratios yields valuable information about the effects of the intersection of different structures and on the pore-water pressure changes in the basin.

5.3. Regional Implications

There is a debate about the age of onset of regional extension in western Anatolia. As mentioned previously, this debate is also related to the origin, mode and controlling factors of extension in the region. Most of the models (references herein) propose that extension commenced some time between the Late Oligocene and Middle Miocene and has continued to Present with (Koçyigit et al., 1999) or without interruption (Seyitoglu and Scott, 1991; Seyitoglu et al., 1992; Isik et al., 2003). Sengör et al. (1985) and Sengör (1987) have proposed that extension in the Aegean region is due to the collision and northwards convergence of Arabian Plate with the Eurasian Plate, resulting in the formation of the North Anatolian and East Anatolian Transform Faults and the westward flight of the Anatolian wedge. Extension in the region commenced at the end of Middle Miocene and has continued to the present time.

The dispute concerning the commencement of extension in western Anatolia results from the scarcity of fossil material, from disputes concerning dating by pollen so that the ages of units are uncertain and from some researchers not taking all the available evidence into account. Generally, the change in depositional styles and the alternation of depositional and erosional periods is attributed to changes in the tectonic configuration in the region. In such interpretations, major eustatic and local (basin scale) controls on erosion and deposition and coupling of sedimentation and tectonics are not taken into consideration.

The recognition of the bimodal direction of extension in the time interval since the Late Miocene and their coincidence with the extension directions measured from actively developing travertine fissures and solutions of earthquake focal mechanisms (Eyidogan and Jackson, 1985; Taymaz et al., 1991; Taymaz and Price, 1992) and GPS velocity vectors (McClusky et al., 2000) indicate that extension in western Anatolia commenced in the Late Miocene and is still active.

6. Conclusions

The following conclusions have been obtained from this study;

1. Denizli Basin is the eastern continuation of the Büyükmenderes and Gediz Grabens, and developed in the area where they interfere.
2. In the Denizli Basin, the orientations of σ_2 for the NE–SW direction of extension and σ_3 orientations of the NW–SE extension direction are almost parallel to each other. This relationship is interpreted as the result of either (favored) stress permutations or of triaxial strain conditions; the latter interpretation is less favored because the structures in the Denizli Basin are generally orthogonal.
3. Age of the basin-filling units of the Denizli Basin are dated by the mammal fauna and range from Early–Middle Miocene to Recent.
4. Early to Middle Miocene units are widespread, while Late Miocene to Recent units are restricted to the Denizli Basin. This is relationship is interpreted to indicate that the deposition of the Early to Middle Miocene units predated the development of the Denizli Basin.
5. Extension in the region commenced in the Late Miocene and has continued, possibly without a break, and is presently active.
6. Local stress magnitude ratios can be plotted using various interpolation techniques. Sharp changes of magnitude may indicate the presence of subsurface structures or regional lineaments, which cannot be recognized directly in the field.
7. The plotting techniques used in this study are not new, but in this study have been applied for the first time in Western Turkey.

Acknowledgements

Hans de Bruijn, Gerçek Saraç, Ercan Sangu helped in sampling for rodents. Hans de Bruijn is also acknowledged for determining the fossils and Erksin Güleç generously supplied her unpublished vertebrate database. The SRTM data was obtained from the USGS website. Arda Arcasoy and Pınar Ertepınar processed the SRTM data. The field data was collected during two periods, in the summers of 2002 and 2004. Ali Koçyigit collaborated in the first part of this study and I have benefited from his ideas. This project is partly supported by the METU Scientific Research Projects Fund.

References

Alessio, M.A., Martel, S.J., 2004. Fault terminations and barriers to fault growth. Journal of Structural Geology 26, 1885–1896.

Altunel, E., Hancock, P.L., 1993. Morphological features and tectonic setting of Quaternary travertines at Pamukkale, western Turkey. Geological Journal 28, 335–346.

André, A-S., Sausse, J., Lespinasse, M., 2001. A new approach for the quantification of paleostress magnitudes: application to the Soultz vein system (Rhine Graben, France). Tectonophysics 336, 215–231.

Angelier, J., 1975. Sur l'analyse de measures recueillies dans des sites faillés: l'utilité d'une confrontation entre les methods dynamiques et cinématiques. Comptes Rendus de l'Académie des Sciences Series D 281, 1805–1808.

Angelier, J., 1984. Tectonic analysis of fault-slip data sets. Journal of Geophysical Research 89, 5835–5848.

Angelier, J., 1989. From orientation to magnitudes in paleostress determination using fault slip data. Journal of Structural Geology 11, 37–50.

Angelier, J., 1990. Inversion of field data in fault tectonics to obtain regional stress. III. A new rapid direct inversion method by analytical means. Geophysical Journal International 103, 363–376.

Angelier, J., 1994. Fault slip analysis and paleostress reconstruction. In: Hancock, P.L. (Ed.), Continental Deformation. Pergamon Press, Oxford, pp. 53–100.

Angelier, J., Tarantola, A., Manoussis, S., Valette, B., 1982. Inversion of field data in fault tectonics to obtain the regional stress. Geophysical Journal of the Royal Astronomical Society 69, 607–621.

Armijo, R., Carey, E., Cisternas, A., 1982. The inverse problem in microtectonics and the separation of tectonic phases. Tectonophysics 82, 145–169.

Arthaud, F., 1969. Méthode de determination graphique des directions de reccourcissement, d'allongement et intermédiaire d'une population de failles. Bulletin de la Societé Géologique de France 7, 729–737.

Bergerat, F., 1987. Stress fields in the European platform at the time of Africa–Eurasia collision. Tectonics 6, 99–132.

Bott, M.P.H., 1959. The mechanics of oblique-slip faulting. Geological Magazine 96, 109–117.

Bozkurt, E., 2000. Timing of extension on the Büyükmenderes Graben, western Turkey, and its tectonic implications. In: Bozkurt, E., Winchester, J.A., Piper, J.D.A. (Eds.), Tectonics and Magmatism in Turkey and the Surrounding Area. Geological Society London, Special Publication 173, pp. 385–403.

Bozkurt, E., 2001. Neotectonics of Turkey—a synthesis. Geodinamica Acta 14, 3–30.

Bozkurt, E., 2003. Origin of NE-trending basins in western Turkey. Geodinamica Acta 16, 61–81.

Bozkurt, E., Park, R.G., 1994. Southern Menderes Massif: an incipient metamorphic core complex in western Anatolia, Turkey. Journal of Geological Society London 151, 213–216.

Carey, E., Brunier, B., 1974. Analyse théorique et numérique d'une modèle méchanique élémentaire appliqué a l'étude d'une population de failles. Comptes Rendus de l'Académie des Sciences Series D 279, 891–894.

Carey-Gailhardis, E., Mercier, J.L., 1987. A numerical method for determining the state of stress using focal mechanisms of earthquake populations: application to Tibetan teleseisms and microseismicity of southern Peru. Earth and Planetary Science Letters 82, 165–179.

Davis, J.C., 2002. Statistics and Data Analysis in Geology, third ed. Wiley, New York, p. 638.

Dewey, J.F., Sengör, A.M.C., 1979. Aegean and surrounding regions: complex multiple and continuum tectonics in a convergent zone. Geological Society America Bulletin 90, 84–92.

Donath, F.A., 1962. Analysis of Basin-Range structure, south-central Oregon. Geological Society America Bulletin 73, 1–16.

Duermeijer, C.E., Nyst, M., Meijer, P.Th., Langereis, C.G., Spakman, W., 2000. Neogene evolution of the Aegean arc: paleomagnetic and geodetic evidence for a rapid and young rotation phase. Earth and Planetary Science Letters 176, 509–525.

Etchecopar, A., Visseur, G., Daignieres, M., 1981. An inverse problem in microtectonics for the determination of stress tensors from fault striation analysis. Journal of Structural Geology 3, 51–65.

Eyidogan, H., Jackson, J.A., 1985. A seismological study of normal faulting in the Demirci, Alasehir and Gediz earthquake of 1969–1970 in western Turkey: implications for the nature and geometry of deformation in the continental crust. Geophysical Journal of Royal Astronomical Society 81, 569–607.

Gephart, J.W., 1990. Stress and direction of slip on fault planes. Tectonophysics 8, 845–858.

Gephart, J.W., Forsyth, D.W., 1984. An improved method for determining the regional stress tensor using earthquake focal mechanism data. Journal of Geophysical Research B89, 9305–9320.

Glover, C., Robertson, A.H.F., 1998. Neotectonic intersection of the Aegean and Cyprus tectonic arcs: extensional and strike–slip faulting in the Isparta Angle, SW Turkey. Tectonophysics 298, 103–132.

Gürer, Ö.F., Kaymakci, N., Çakır, S., Özburan, M., 2003. Neotectonics of Southeast Marmara Region (NW Anatolia Turkey). Asian Journal of Earth Sciences 21, 1041–1051.

Hancock, P.L., 1985. Brittle microtectonics: principles and practice. Journal of Structural Geology 7, 437–457.

Hancock, P.L., Altunel, E., 1997. Faulted archeological relics at Hieropolis (Pamukkale). Turkey. Journal of Geodynamics 24, 21–36.

Hancock, P.L., Chalmers, R.M.L., Altunel, E., Çakır, Z., 1999. Travitonics: using travertines in active fault studies. Journal of Structural Geology 21, 903–916.

Hardcastle, K.C., Hills, L.S., 1991. BRUTE3 and SELECT: QuickBasic 4 programs for determination of stress tensor configurations and separation of heterogeneous populations of fault–slip data. Computers & Geosciences 17, 23–43.

Homberg, C., Hu, J.C., Angelier, J., Bergerat, F., Lacombe, O., 1997. Characterization of stress perturbation near major fault zones: insights from 2-D distinct-element numerical modelling and field studies (Jura Mountains). Journal of Structural Geology 19, 703–718.

Homberg, C., Angelier, J., Bergerat, F., Lacombe, L., 2004. Using stress directions to identify slip events in fault systems. Earth and Planetary Science Letters 217, 409–424.

Isik, U., Seyitolu, G., Cemen, I., 2003. Ductile–brittle transition along the Alosehir shear zone and its structural relationship with the Simav detachment, Menderes Massif, western Turkey. Tectnophysics 374, 1–18.

Jackson, J.A., McKenzie, D.P., 1984. Active tectonics of the Alpine–Himalayan Belt between western Turkey and Pakistan. Geophysical Journal of the Royal Astronomical Society 7, 185–264.

Jaeger, J.C., Cook, N.G.W., 1969. Fundamentals of Rock Mechanics. Methuen, London.

Kaymakci, N., 2000. Tectono-stratigraphical evolution of the Çankiri Basin (Central Anatolia, Turkey). PhD Thesis, Utrecht University, The Netherlands. Geologica Ultraiectina No. 190, 248 pp.

Kaymakci, N., White, S.H., van Dijk, P.M., 2000. Paleostress inversion in a multi-phase deformed area: kinematic and structural evolution of the Çankırı Basin (Central Turkey): Part 1. In: Bozkurt, E., Winchester, J.A., Piper, J. (Eds.), Tectonics and Magmatism in Turkey and its Surroundings. Geological Society London, Special Publication 173, pp. 445–473.

Kaymakci, N., Duermeijer, C.E., Langereis, C., White, S.H., van Dijk, P.M., 2003a. Oroclinal bending due to indentation: a paleomagnetic study for the early Tertiary evolution of the Çankırı Basin (Central Anatolia Turkey). Geological Magazine 140, 343–355.

Kaymakci, N., White, S.H., van Dijk, P.M., 2003b. Kinematic and structural development of the Çankırı Basin (Central Anatolia Turkey): a paleostress inversion study. Tectonophysics 364, 85–113.

Koçyigit, A., Yusufoglu, H., Bozkurt, E., 1999. Evidence from the Gediz Graben for episodic two-stage extension in western Turkey. Journal of Geological Society London 156, 605–616.

Kokkalas, S., Doutsos, T., 2001. Strain-dependent stress field and plate motions in the south-east Aegean region. Journal of Geodynamics 32, 311–332.

Krantz, R.W., 1988. Multiple fault sets and three-dimensional strain: theory and application. Journal of Structural Geology 10, 225–237.

Le Pichon, X., Angelier, J., 1979. The Aegean arc and trench system: a key to the neotectonic evolution of the Eastern Mediterranean area. Tectonophysics 60, 1–42.

Lee, J.-C., Angelier, J., 1994. Paleostress trajectory maps based on the results of local determinations: the 'Lissage' program. Computers & Geosciences 20, 161–191.

Lips, A.L.W., 1998. Temporal constraints on the kinematics of the destabilization of an orogen: syn-to post-orogenic extensional collapse of the Northern Aegean region. PhD Thesis, Utrecht University, The Netherlands. Geologica Ultraiectina No.166, 222 pp.

Lips, A.L.W., Cassard, D., Sözbilir, H., Yılmaz, Y., 2001. Multistage exhumation of the Menderes Massif, western Anatolia (Turkey). International Journal of Earth Sciences 89, 781–792.

Marrett, R., Almandinger, R.W., 1990. Kinematic analysis of fault slip data. Journal of Structural Geology 12, 973–986.

McClusky, S.C., Balassanian, S., Barka, A.A., Demir, C., Ergintav, S., Georgiev, L., Gürkan, O., Hamburger, M., Hurst, K., Kahle, H.G., Kastens, K., Kekelidze, G., King, R., Kotzev, V., Lenk, O., Mahmoud, S., Mishin, A., Nadariya, M., Ouzounis, A., Paradissis, D., Peter, Y., Prilepin, M., Reilinger, R.E., Sanlı, I., Seeger, H., Tealeb, A., Toksöz, M.N., Veis, G., 2000. Global positioning system constraints on plate kinematics and dynamics in the Eastern Mediterranean and Caucasus. Journal of Geophysical Research 105, 5695–5720.

Michael, A.J., 1984. Determination of stress from slip data: faults and folds. Journal of Geophysical Research B89, 11517–11526.

Nemcok, M., Lisle, R.J., 1997. A stress inversion procedure for polyphase fault/slip data sets. Journal of Structural Geology 17, 1445–1453.

Pollard, D.D., Saltzer, S.D., Rubin, A.M., 1993. Stress inversion methods: are they based on faulty assumptions? Journal of Structural Geology 15, 145–154.

Provost, A-S., Chéry, J., Hassani, R., 2003. 3D mechanical modeling of the GPS velocity field along the North Anatolian fault. Earth and Planetary Science Letters 209, 361–377.

Ramsay, J.G., Lisle, R.J., 2000. The techniques of modern structural geology. Applications of Continuum Mechanics in Structural Geology, vol. 3. Academic Press, London.

Reches, Z., 1978. Analysis of faulting in three-dimensional strain field. Tectonophysics 47, 109–129.

Reches, Z., 1987. Determination of the tectonic stress tensor from slip along faults that obey the Coloumb yield criterion. Tectonics 6, 849–861.

Reilinger, R.E., McClusky, S.C., 2001. GPS constraints on block motions in western Turkey and the Aegean: implications for earthquake hazards. Proceedings of Symposium on Seismotectonics of the NW Anatolia-Aegean and Recent Turkey Earthquakes. May 8, 2001. Istanbul Technical University (ITÜ), Istanbul, 14–20.

Saraç, G., Güleç, E., de Bruijn, H., Howell, C., White, T., Sevim, A., van Meulen, A., 2001. Türkiye omurgalı Fosil Yatakları. MTA Genel MüdürlŸgü, Raporu, 169s. (Yayimlanmamis).

Sengör, A.M.C., 1987. Cross-faults and differential stretching of hanging walls in regions of low-angle normal faulting: examples from western Turkey. In: Coward, M.P., Dewey, J.F., Hancock, P.L. (Eds.), Continental Extensional Tectonics. Geological Society London, Special Publications 28, pp. 575–589.

Sengör, A.M.C., Saroglu, F., Görür, N., 1985. Strike-slip deformation and related basin formation in zones of tectonic escape: Turkey as a case study. In: Biddle, K.T., Christie-Blick, N. (Eds.), Strike–Slip Deformation Basin Formation and Sedimentation Society of Economic Palaeontologists and Mineralogists. Special Publication 37, pp. 227–264.

Seyitoglu, G., Scott, B.C., 1991. Late Cenozoic crustal extension and basin formation in west Turkey. Geological Magazine 128, 155–166.

Seyitoglu, G., Scott, B.C., 1996. The cause of N–S extensional tectonics in western Turkey: tectonic escape vs back-arc spreading vs. orogenic collapse. Journal of Geodynamics 22, 145–153.

Seyitoglu, G., Scott, B.C., Rundle, C.C., 1992. Timing of Cenozoic extensional tectonics in west Turkey. Journal of Geological Society London 149, 533–538.

Straub, C., Kahle, H.-G., Schindler, C., 1997. GPS and geologic estimates of the tectonic activity in the Marmara Sea region, NW Anatolia. Journal of Geophysical Research 102, 27587–27601.

Taymaz, T., Price, S., 1992. The 1971 May 12 Burdur Earthquake sequence, SW Turkey—a synthesis of seismological and geological observations. Geophysical Journal International 108, 589–603.

Taymaz, T., Jackson, J.A., McKenzie, D.P., 1991. Active tectonics of the north and central Aegean Sea. Geophysical Journal International 106, 433–490.

Ten Veen, J.H., Kleinspehn, K.L., 2003. Incipient continental collision and plate-boundary curvature: Late Pliocene–Holocene transtensional Hellenic forearc, Crete, Greece. Journal of Geological Society London 160, 161–181.

Toprak, V., Kaymakci, N., 1995. Characteristics of the Derinkuyu Fault in Central Anatolia: a paleostress inversion study. Turkey Journal of Earth Sciences 5, 21–29.

Treagus, S.H., Lisle, R., 1997. Do principal surfaces of stress and strain always exist? Journal of Structural Geology 19, 997–1010.

Twiss, R.J., Unruh, J.R., 1998. Analysis of fault slip inversion: do they constrain stress or strain rate? Journal of Geophysical Research 103 (B6), 12205–12222.

Walcott, C.R., White, S.H., 1998. Constraints on the kinematics of post-orogenic extension imposed by stretching lineations in the Aegean region. Tectonophysics 298, 155–175.

Wallace, R.E., 1951. Geometry of shearing stress and relation to faulting. Journal of Geology 69, 118–130.

Westaway, R., 1994. Evidence for dynamic coupling of surface processes with isostatic compensation in the lower crust during active extension of western Turkey. Journal of Geophysical Research 99, 20203–20223.

Will, T.M., Powel, R., 1991. A robust approach to the calculation of paleostress fields from fault plane data. Journal of Structural Geology 13, 813–821.

Yin, Z.M., Ranalli, G., 1993. Determination of tectonic stress field from fault slip data, toward a probabilistic model. Journal of Geophysical Research 98, 12165–12176.